

# Aeroradiometric Data Assessment of Hydrothermal Alteration Zones in Parts of North Central Nigeria

Mam D. Tawey<sup>1\*</sup>, Abbass A. Adetona<sup>2</sup>, Usman D. Alhassan<sup>2</sup>,  
Abdulwaheed A. Rafiu<sup>2</sup>, Kazeem A. Salako<sup>2</sup> and Emmanuel E. Udensi<sup>2</sup>

<sup>1</sup>National Water Resources Institute, Mando Road Kaduna, Nigeria.

<sup>2</sup>Geophysics Department Federal University of Technology Minna, Nigeria.

## **Authors' contributions**

*This work was carried out in collaboration among all authors. Author MDT designed the study, performed the statistical analysis, wrote the protocol and wrote the first draft of the manuscript. Authors AAA, UDA and AAR managed the analyses of the study. Authors KAS and EEU managed the literature searches. All authors read and approved the final manuscript.*

## **Article Information**

### Editor(s):

(1) Dr. Adewumi, Adeniyi JohnPaul, Achievers University, Nigeria.

### Reviewers:

(1) S.Periyasamy, Anna University, India.

(2) I. Aswin Kumar, Czech Technical University in Prague, Czech Republic.

Complete Peer review History: <http://www.sdiarticle4.com/review-history/67062>

**Original Research Article**

**Received 13 February 2021**

**Accepted 23 April 2021**

**Published 30 April 2021**

## **ABSTRACT**

This work aims to map radioelement distribution, delineate hydrothermal alteration areas, and produce a surface geologic map of the area using recently acquired high-resolution aeroradiometric data covering parts of north-central Nigeria with estimated area coverage of 24, 200 Km<sup>2</sup>. Radioelement maps, ratio maps, and composite radioelement maps were produced to accomplish this goal. The spatial distribution and occurrence of each radioelement were determined using the radioelement maps, and hydrothermal alteration zones that fell within the north, northeast, northwest, southwest, and eastern portions of the study area were delineated using the percentage potassium (% K)-equivalent Thorium (eTh) ratio (K/eTh) map. Some of these altered zones have one or more structural associations, implying that the structures serve as channels (pathways) for migrating hydrothermal fluids that reacted with rock formations that were later altered. The coincidences in these alteration zones with high lineaments densities areas discovered by previous work in this area suggest a high likelihood of the occurrence of prospective mineralization within these locations. The composite maps aided in the production of the study

\*Corresponding author: Email: [taweymam@gmail.com](mailto:taweymam@gmail.com);

area's surface geology map, while the paleostructure trending NE-SE revealed in previous work within the study area based on aeromagnetic data analysis was delineated using both radioelement and composite radioelement (ternary) maps.

*Keywords: Hydrothermal; alteration; mineralization; structures and radioelement.*

## 1. INTRODUCTION

Radiometric surveys are a rapid and powerful tool providing information about the distribution and concentration of uranium (U), thorium (Th), and potassium (K). Aside from determining the radiogenic heat production of rocks, they have a variety of applications ranging from geological and geochemical mapping to the discovery of radioactive mineral resources and environmental studies for radon risk assessment [1]. It has recently been used in geologic structural studies [2,3]. These structures play important roles in the localisation of mineralization zones. Also, high-resolution airborne geophysical data shows usefulness as high-quality approaches that allow extracting geological information from data and are used as an aid to lithological mapping [4]. This technique is cost-effective and rapid for geochemical mapping of the radioactive elements: potassium, uranium and thorium. Also, the gamma-ray spectrometric method shows more success in mapping surface geology. [5,6] showed in their work that potassium concentrations were higher in mineralized zones than in non-mineralized areas, by up to a factor of two, and showed a zonal distribution related to the ore deposits. During magmatic differentiation, potassium is gradually concentrated so that more potassium is concentrated in felsic rocks than mafic igneous rocks. This is observed in variations in basalt K concentration, normally less than 1%, and granite, which is 2% to less than 6% [7 – 9]. [10] indicated that the main sources of potassium are destroyed during weathering process in the order of biotite-K-feldspar-muscovite. A decrease in Th and an increase in K are indicative of an ore deposit's alteration environments [11]. Thorium generally is not affected by alteration processes because Th is typically immobile in mineralization processes or it can only partly be depleted in areas of intense K-alteration and silicification. The K/Th ratio is therefore a better indicator of hydrothermal alteration than any single radioelement alone. The concentration of soil clay and silt are also characterized by thorium and Th/K [12, 13].

[1, 10 & 14] stated that in some gold deposits, Th has been mobilized and depleted while K has increased even though Th is generally unaffected by alteration processes. Potassium anomalies across the ore deposits are fairly well known by standard geochemical studies and potassium metasomatism according to [14], suggesting that potassium is the most effective pathfinder Element [10]. Alterations, weathering, climatic conditions, and hydrothermal processes can affect the radioelement concentration [15]. Hydrothermal processes may lead to variations in the content of host rocks' radioelements. K is often affected by these processes among the three radioelements, Th less frequently and U quite infrequently. Potassium often increases during signature alterations but weathering usually decreases the intensity of signature alterations. Potassium is generally added to the source rocks by mineralizing hydrothermal fluids. It may be hosted by K-feldspar or muscovite and potential outcropping or sub-cropping mineralization can be recognized by an increase in K counts during radiometric surveying [10].

[16] also presented results of ground spectrometry and chemical analyses from copper and copper lead- zinc deposits which showed that potassium concentrations are increased in zones of alteration. Thorium concentrations remained unchanged so that high potassium/thorium values were indicative of the zones of hydrothermal alteration. [17] presented some examples of airborne gamma-ray spectrometry hydrothermal mineralization. Different examples showed mineralization coincident with zones of high uranium/thorium "or high potassium/uranium ratios. Anomalous indications of all these radioelements can define hydrothermal dispersion patterns.

Several studies have also been conducted for identifying alteration zones e.g. [18 – 23]. The present study is aimed at mapping radioelement distribution, delineation of hydrothermal alteration zones and also producing a surface geologic map of the study area.

### 1.1 Location

The research area is bordered by latitudes  $08^{\circ} 30' N$  and  $10^{\circ} 30' N$  and longitudes  $07^{\circ} 00' E$  and  $08^{\circ} 00' E$  and falls within three states in Nigeria (Kaduna, Niger, Nasarawa) and the Federal Capital Territory (Fig. 1). The research area also forms part of the Nigerian schist belt and the younger granite province of Northern Nigeria (Fig. 2). Analysis of digital elevation model (DEM) of the area provided by Shuttle Radar Topography Mission (SRTM), data map (Fig. 3) of the study area showed that topography within the area varied from 116 m for low elevated areas to 986 m for very high elevated areas.

### 1.2 Geology and Tectonic Settings

The Nigerian Basement complex comprises of four major petro-lithological units, namely: Migmatite – Gneiss Complex (MGC), Schist Belt (Metasedimentary and Metavolcanic rocks), Older Granites (Pan African granitoid) and Undeformed Acid and Basic Dykes [24,25].

Within the study area, Migmatites are the most predominant rock types with the schists (undifferentiated schist including phyllites that occur around the north-western and eastern part

of the study area and the Pelitic/Muscovite schists that occur around the southwestern part of the map).

Other rock types are undifferentiated older granites, dolerites, porphyritic granite, granite and granite porphyry, granite gneiss, Medium to coarse-grained biotite granite, Banded gneiss, Migmatitic gneiss and biotite granites (Fig. 4). The study area forms part of north-central Nigerian basement complex that is tectonically part of the Pan-African mobile belt and lies between the West African and Congo Cratons and south of the Tuareg Shield [26].

The study area has been subjected to multiple tectonic movements, resulting in the area being dissected by various forms of faults and joints, all of which are the product of either pre-Pan-African or Pan-African tectonic activity. According to [27], there are observed structures with high lineament densities around the central portion of the study area and span towards the western end of the map (Fig. 5). Structural analysis of aeromagnetic data as delineated from source edge enhancement techniques revealed five tectonic structural trends in the directions ENE-WSW, NE-SW, NNE-SSW, NNW-SSE and WNW-ESE with ENE-WSW being the predominant or major structural trend [27].

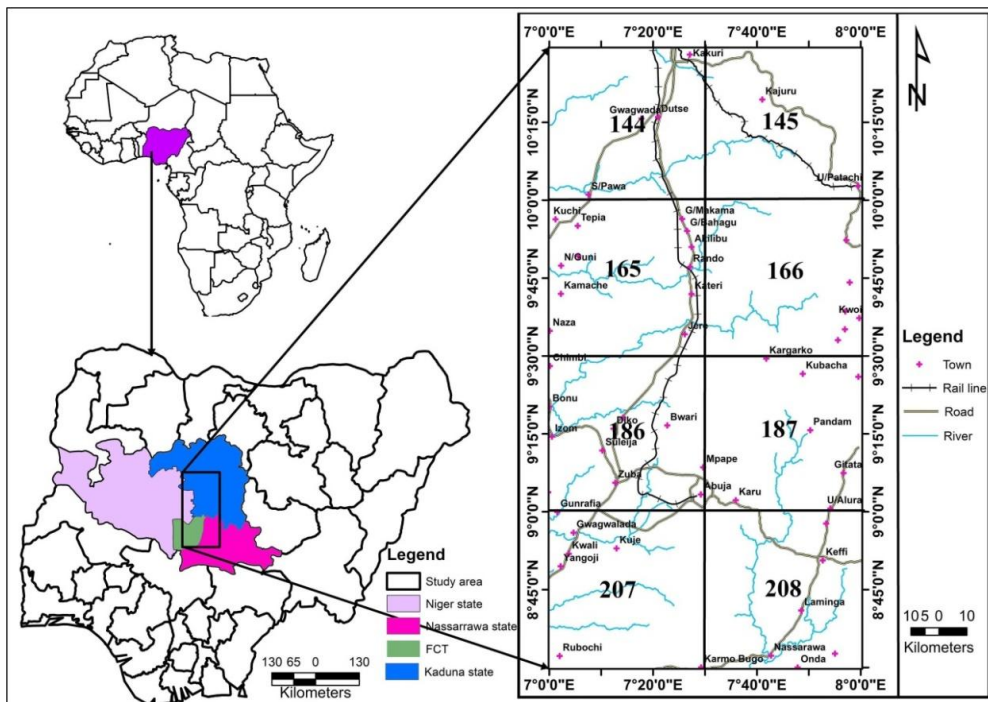


Fig. 1. Location Map of the Study Area

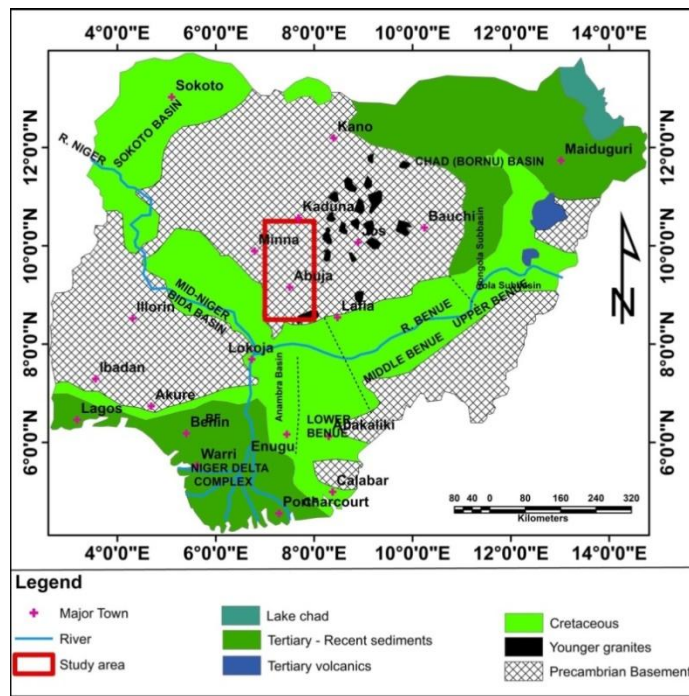


Fig. 2. Generalized Geologic Map of Nigeria

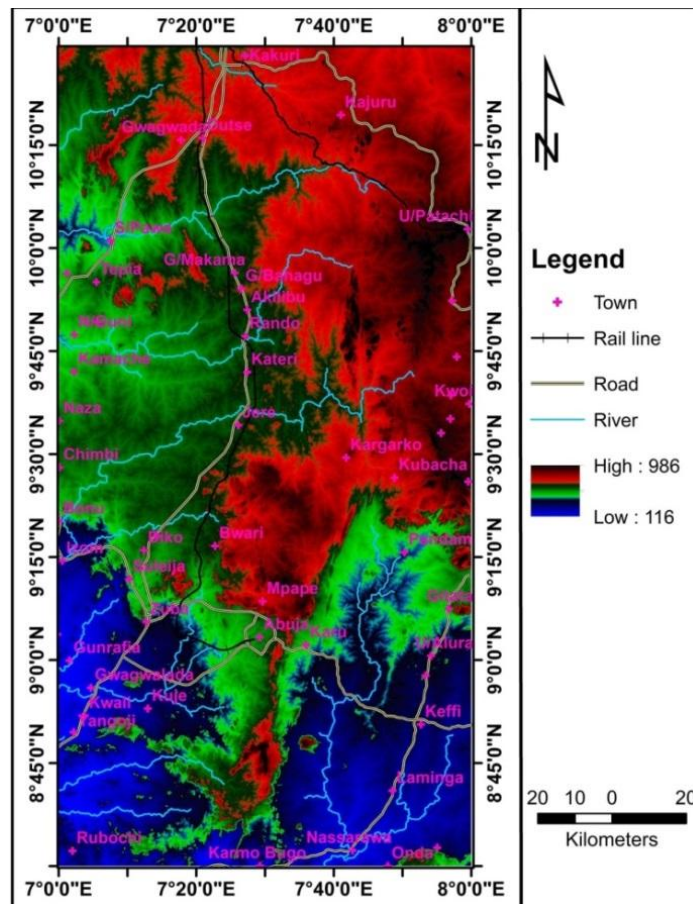


Fig. 3. SRTM DEM Showing Topographic Variation

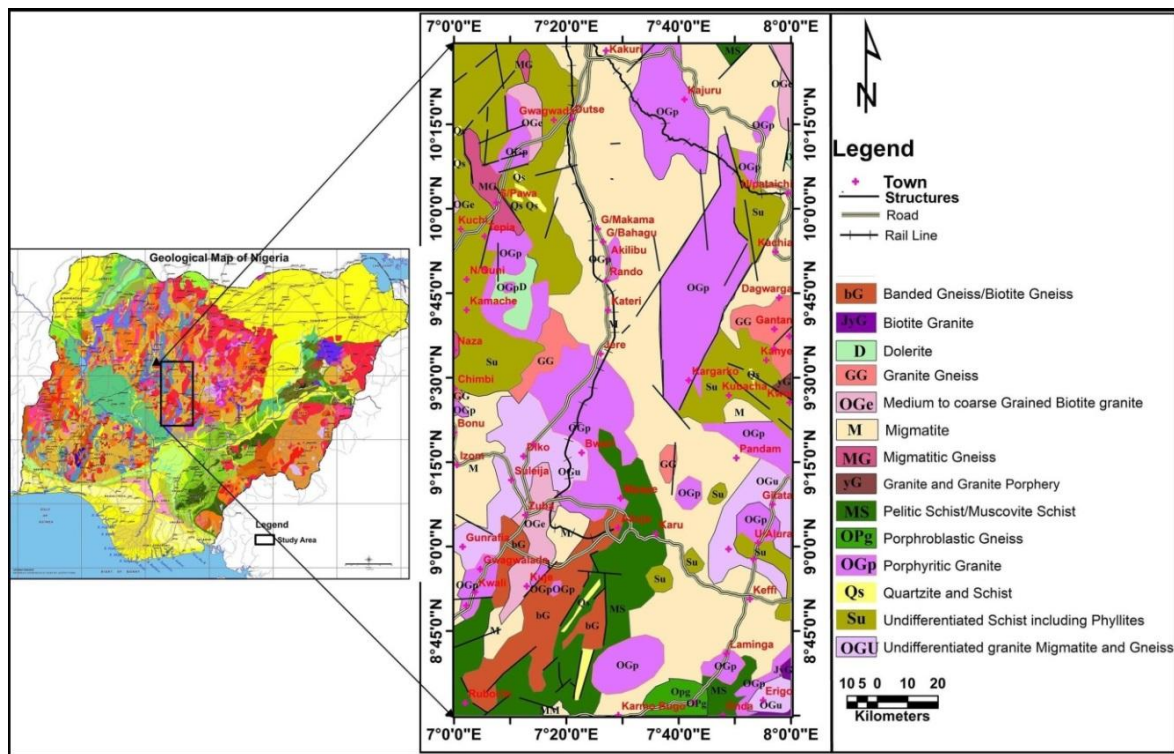


Fig. 4. Geology of the study area

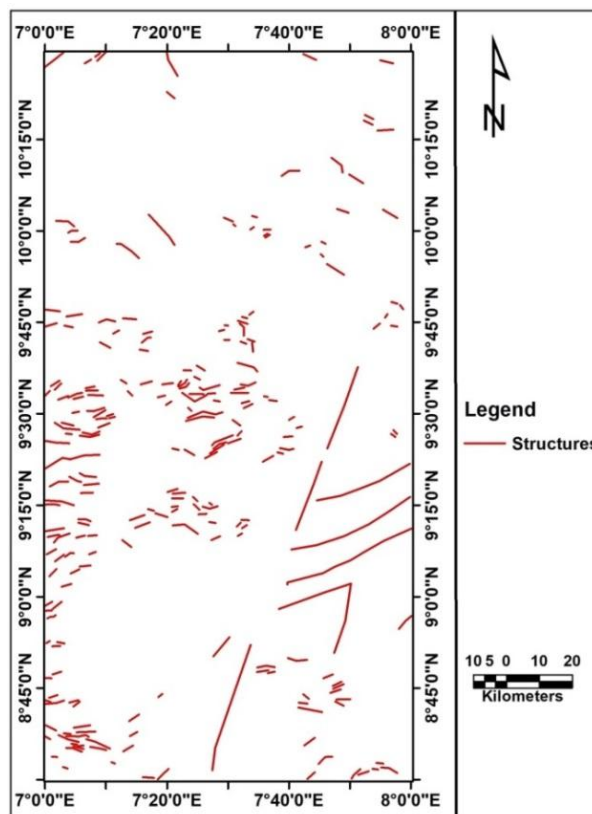


Fig. 5. Structural Map of the Study Area from Analysis of Aeromagnetic Data (Adapted from [27])

## 2. MATERIALS AND METHODS

### 2.1 Data Source

The aeroradiometric data used for this study was acquired from the Nigerian Geological Survey Agency (NGSA) Abuja and consists of sheets (144 Kakuri, 145 Kajuru, 165 Bishini, 166 Kachia, 186 Abuja, 187 Gitata, 207 Kuje and 208 Keffi). The survey was conducted in 2009 and was financed by the Nigerian Federal Government and the World Bank. The survey which was carried out in two phases was fund completely by the Government of Nigeria during the first phase while the second phase was fund by both the Nigerian Government and the World Bank. Fugro Airborne Surveys carried out all the acquisition, processing and analysis of airborne geophysical data.

### 2.2 Methodology

To display the three primary variables measured, three maps were produced: percentage potassium (%K), equivalent Uranium (eU), and equivalent Thorium (eTh). Six other derived products were also useful, including a K/eTh map, ternary K-eU-eTh radioelement maps in Red-Green-Blue and Cyan-Magenta-Yellow (RGB and CYM), and composite radioelement maps.

The resulting images comprise colors generated from the relative intensities of the three components and represent subtle variations in the ratios of the three bands. A histogram equalization to give the best color variation was used to enhance the contrast of the individual histograms of K, Th and U before combining them to the composite image. Since particular rock types often have characteristic ratios of the three radioactive elements, the ternary maps of these ratios are useful geological and mineral exploration tool for discriminating the zones of consistent lithology and contacts between contrasting lithologies[28]. The four composite color images (maps) that were prepared from their respective ratios are as follows:

- i. K, eU and eTh (three radioelements composite image map),
- ii. K, K/eU and K/eTh (potassium composite image map),

- iii. eU, eU/eTh and eU/K (equivalent uranium composite image map),
- iv. eTh, eTh/eU and eTh/K (equivalent thorium composite image map),

Different rock types show different characteristic concentrations of the three main radioelements. Three radioelements composite image map is produced by using different ink colors to represent the K (in per cent), eU (in ppm) and eTh (in ppm) concentrations. At any location, the relative concentrations of the three radioelements are represented by the color hue produced by mixing appropriate amounts of the three ink colors [29,30]. Since a distinct color hue is used to represent each ternary ratio on the map, zones with similar ratios will be represented by a unique color. This distinct relationship between color hue and ternary ratio allows the map to display surface radioelement distribution.

## 3. RESULTS AND DISCUSSIONS

### 3.1 Potassium (%K) Map

The potassium (%K), map (Fig. 6a) shows different degrees of potassium concentrations ranging from 0.178 to 5.340 % that reflects different lithological units and alterations in the area while (Fig. 6b) represent the potassium (%K), map with geology to know the boundary of anomaly source rocks. Alteration, weathering, climatic conditions and hydrothermal processes can affect the concentration of the radioelements [15]. Potassium often increases during signature alterations[31], but weathering usually decreases the intensity of signature alterations[10]. Several potassium anomalies are evident in the radiometric image (Fig. 6a). The color blue corresponds with low K values whilst pink corresponds with very high K values. The color red represents moderately high to high K values and the shades of orange to yellow color represent or are associated with moderately low K values. These pinkish colorations with very high K values are observed in areas around West of Gwagwada in the northwestern part of the study area; east and south of Kajuru in the north-east, East of Pandam, Gitata, north and south of Bwari have high K concentration (Fig. 6a). Also, areas around Karmo, Bugo and Onda in the south showed a high concentration of potassium anomaly.

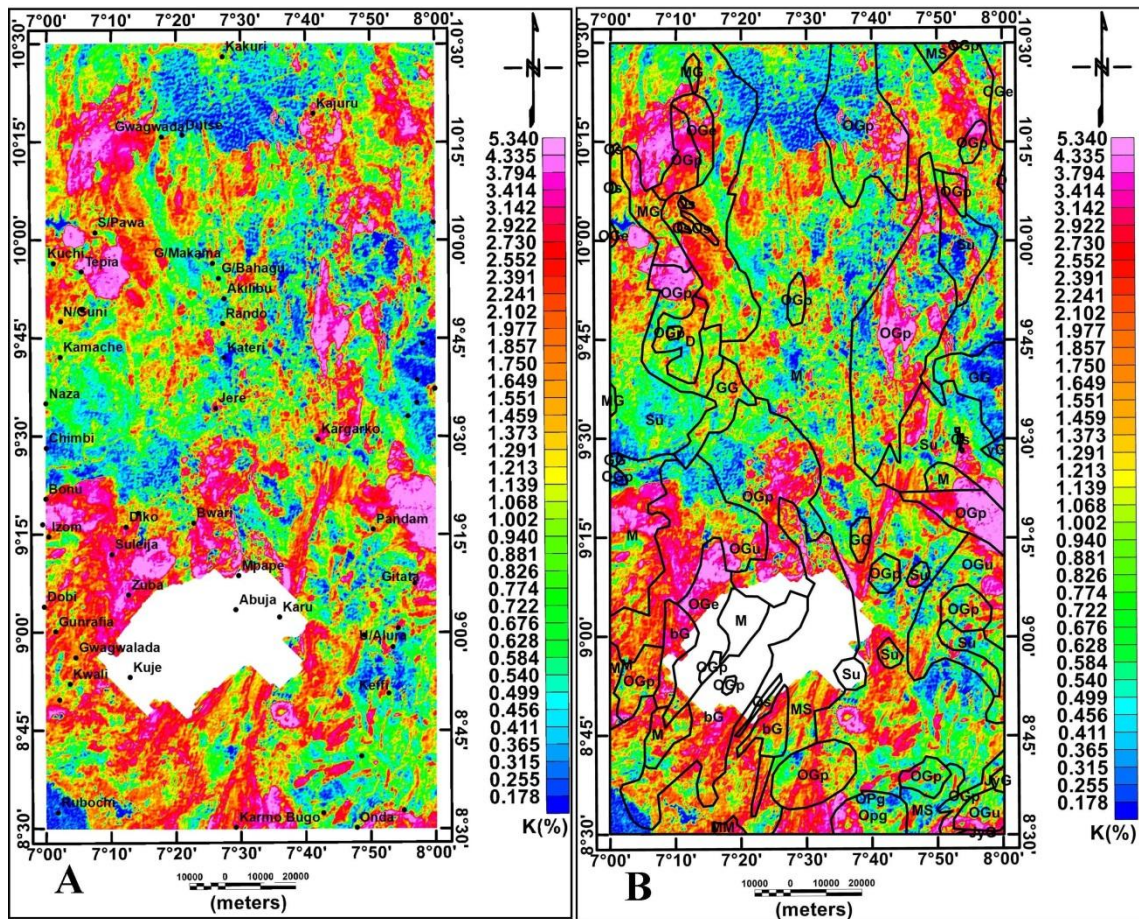


**Fig. 6. a. Potassium (%K) Map and b. Potassium (%K) Map with geology**

(M = Migmatites, Su = Undifferentiated schist including phyllites, MS = Pelitic/Muscovite schists, OGu = Undifferentiated older granites, D = dolerites, OGp = porphyritic granite, yG = granite and granite porphyry, GG = granite gneiss, OGe = Medium to coarse grained biotite granite, bG = Banded gneiss, MG = migmatitic gneiss and JyG = Biotite granites)

Also observed within the K concentration map (Fig. 6a) is a feature having a linear (sheet-like) concentration of K along a suspected fault line that has been delineated on a structural map of the area (Fig. 5) is also observed in K map cutting across the map from south of latitude 10° at the eastern end of the map through the west of Kagarko, Karu to the west of Karmo in the southern end of the map (Fig. 6a). The areas with high K concentrations are attributed to the Pan African Older Granitoids in the area (Biotite granite, undifferentiated granite, medium to coarse-grained Biotite Granite, Granite and Granite porphyry) and the Metasedimentary/Metavolcanic in the area (Pelitic/Muscovite Schists, undifferentiated Schist including Phyllites, Granite Gneiss and Migmatite and granite gneiss) as in (Fig 6b). As pointed out by [7 – 9] , during magmatic differentiation, potassium is concentrated in felsic igneous rocks

than the mafic igneous rocks but this is not the case in the study area as some part of the granitic rocks are showing low potassium concentration which could be attributed to the destruction of potassium source during weathering processes[10].

### 3.2 Thorium (eTh) Map

Thorium generally is not affected by alteration processes because Th is typically immobile in mineralization processes or it can only partly be depleted in areas of intense K-alteration and silicification however, (Fig. 7a) displays the eTh distribution map of the study area while (Fig. 7b) displays eTh distribution map of the study area overlaid with geology. The eTh distribution map has eTh concentration ranging from 6.822 to 65.739 ppm. For this interpretation, the eTh concentration in the study area will be relatively

grouped as high (>28.823 ppm), moderately high (16.674–28.823ppm), moderately low (10.842–16.674 ppm), and low (<10.842ppm). The high concentrations in eTh marked by red to pink colorations are observed in the north, from the northern edge of the study area through Kakuri down to north of Jere also from east of Kajuru to the north-eastern edge of the map (Fig. 7a). The high concentration of eTh is also observed in areas around the south of Onda, Rubochi and north of Gunrafia. Also observed within the eTh concentration map (Fig. 7a) as observed within the K concentration map (Fig. 6a) is a feature having a linear (sheet-like) concentration of K along the suspected fault line that has been delineated on FVD map (Fig. 5). Areas of high eTh concentrations are attributed to the Pan African Older Granitoids in the area (Biotite and granite, undifferentiated granite, Biotite Granite, medium to coarse-grained Biotite Granite, Granite and Granite porphyry) and the

Metasedimentary/Metavolcanic in the area (Pelitic/Muscovite schists, undifferentiated Schist including Phyllites, Granite Gneiss and Migmatite and granite gneiss).

### 3.3 Uranium (eU) Map

Fig. 8a. displays the eU concentration map while (Fig.8b) displays the eU concentration map with the geology of the study area and according to [32], Uranium is a very mobile element in hydrothermal and other geological processes; an enrichment of uranium may or may not be accompanied by an enrichment of potassium. The map (Fig. 8a) shows various anomalous signatures with total eU concentrations varying between 1.236 ppm to 15.780 ppm. The eU concentrations can be relatively grouped as high (>6.943), moderately high (4.122–6.943), moderately low (2.618-4.122) and low (< 2.618). Just as observed within the structural map

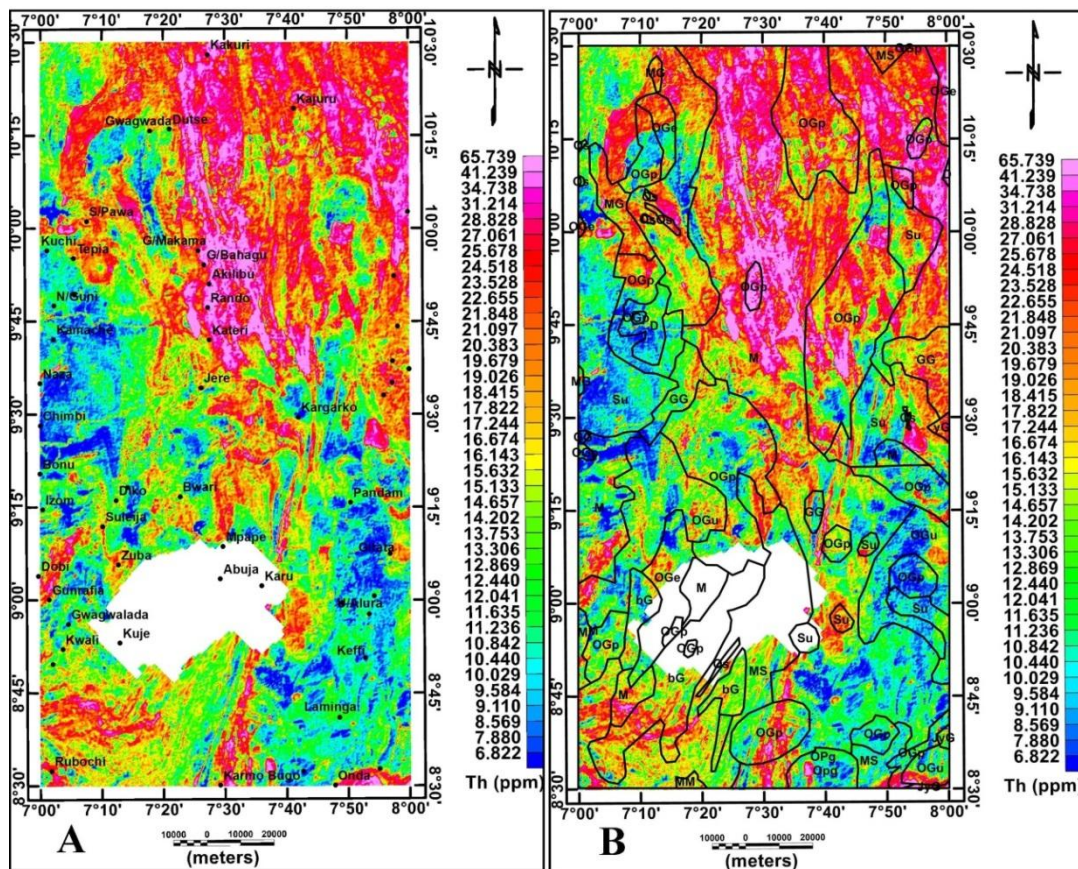


**Fig. 7. a. eTh (ppm) Map and b. eTh (ppm) map with Geology**

(M = Migmatites, Su = Undifferentiated schist including phyllites, MS =Pelitic/Muscovite schists, OGu= Undifferentiated older granites, D = dolerites, OGp = porphyritic granite, yG = granite and granite porphyry, GG= granite gneiss, OGe = Medium to coarse grained biotite granite, bG= Banded gneiss, MG = migmatitic gneiss and JyG = Biotite granites)



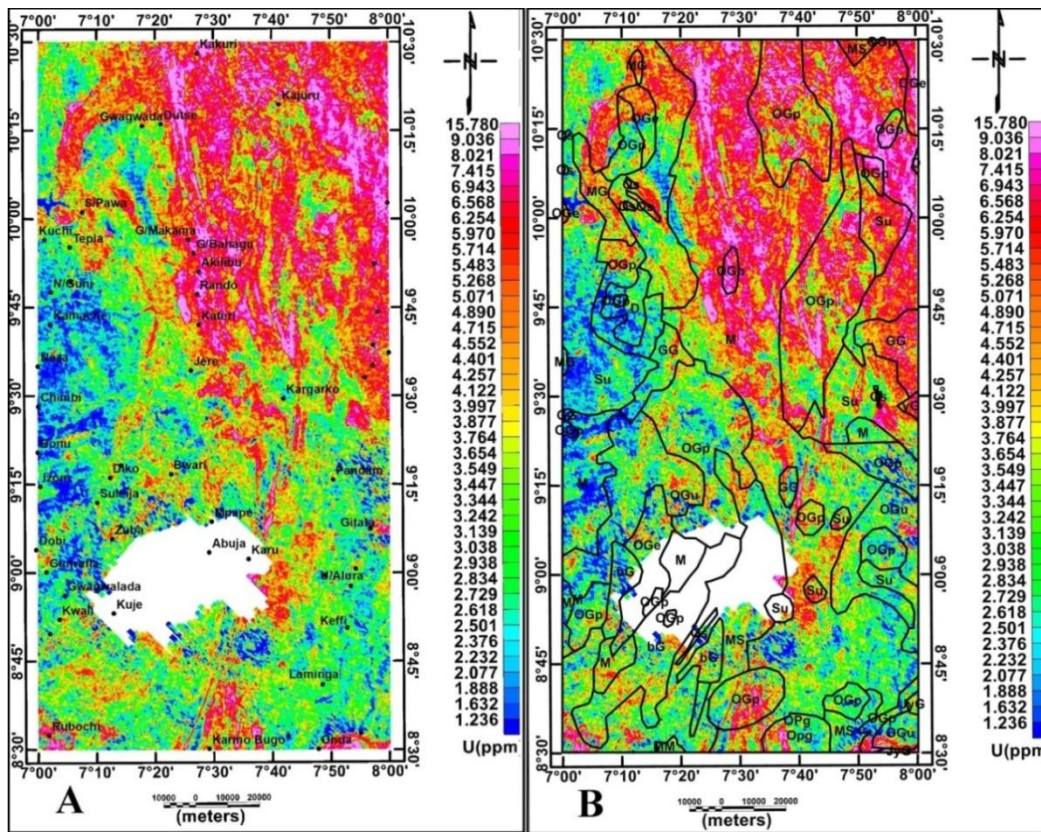


**Fig. 8. a. Uranium (eU) Concentration Map and b. Uranium (eU) Concentration Map with Geology**

(M = Migmatites, Su = Undifferentiated schist including phyllites, MS = Pelitic/Muscovite schists, OGu = Undifferentiated older granites, D = dolerites, OGp = porphyritic granite, yG = granite and granite porphyry, GG = granite gneiss, OGe = Medium to coarse grained biotite granite, bG = Banded gneiss, MG = migmatitic gneiss and JyG = Biotite granites)

(Fig. 5), K (%) and eTh concentration maps (Fig. 6a and Fig. 7a) that displays linear (sheet-like) concentration of K (%) and eTh also occur in eU map (Fig. 8a). Also, areas of high eU concentrations just as eTh map are attributed to the Pan African Older Granitoids in the area (Undifferentiated granite, Biotite Granite, medium to coarse-grained Biotite Granite, Granite and Granite porphyry) and the Metasedimentary/Metavolcanic in the area (Pelitic/Muscovite schist, undifferentiated Schist including Phyllites, Granite Gneiss and Migmatite and granite gneiss).

### 3.4 Ratio Maps

Fig. 9a. display %K/eTh map and as potassium is more mobile than thorium, K/eTh ratio anomalies can be distinguished to areas of hydrothermal alteration which are characterized

by K enrichment. However, depending on the fact that the ratio between potassium and thorium is rather constant in most rocks, typically varying from 0.17 to 0.2 (K/Th in %/ppm, [14]). Rocks with K/eTh ratios remarkably outside of this range have been named potassium or thorium specialized [33].

So, the zones characterized by the high K/eTh ratio values are the strong indicator of hydrothermal alteration. From the K/eTh ratio map (Fig. 9a) it is seen that the areas affected by the hydrothermal process are featured by pink color and have a high value of about 0.635 of K/eTh ratio. From (Fig. 9b) alteration zones fall within the schists, medium to coarse-grained biotite granite at the northwestern portion of the map. This is also observed within the migmatite the western edge and southeastern portion of the map.

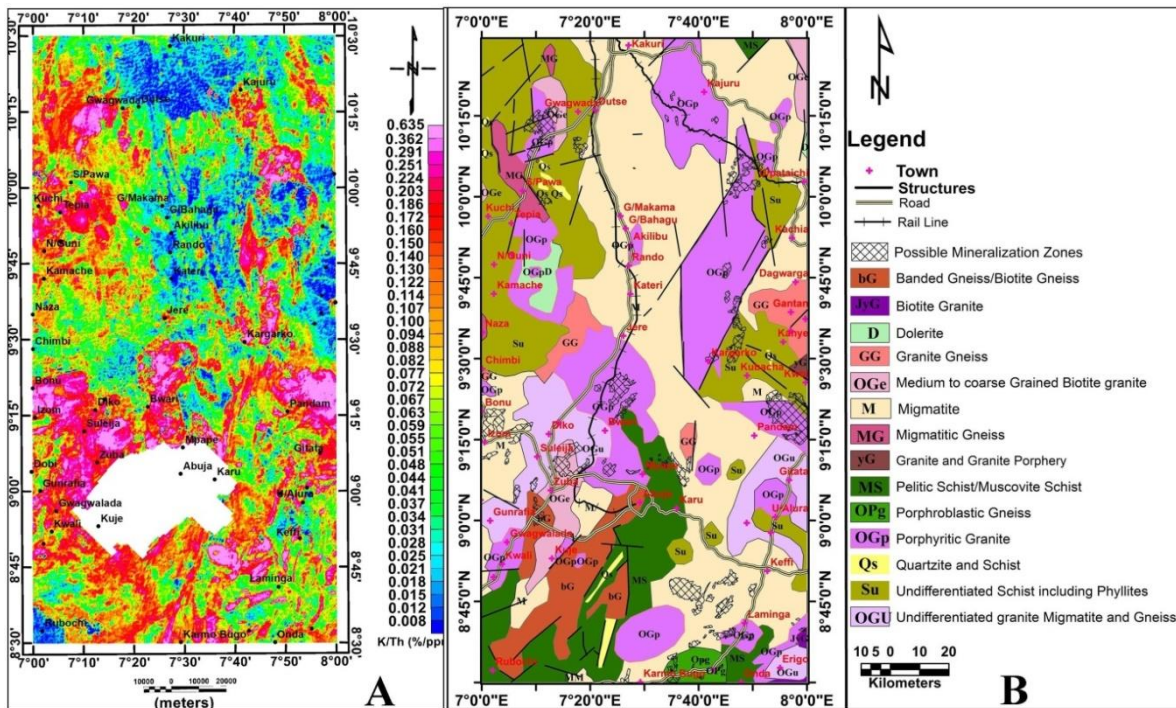


Fig. 9. a. Potassium/Thorium (%/ppm) Ratio Map and b. Hydrothermal Alteration Zones on Geologic Map of the Area

### 3.5 Ternary Maps

In the RGB ternary map (Fig. 10a) while (Fig. 10b) is the CMY ternary map produced to compliment the RGB ternary map for geological mapping which in turn found to be very useful for anomaly discrimination. Bright blue parts on the RGB ternary map show zones, where the uranium count rate is very high relative to both of the other element count rates, bright Red indicates zones of high potassium count rate, and bright green indicates zones of high thorium count rate. Colors other than the three primary colors indicate zones with various well-defined proportions of Th, U and K. Generally, the different colors on the ternary map correspond closely with different rock types when compared with the geological map. Taking into consideration the geology of the area early mentioned (Fig. 4) and the gamma-ray spectrometric response shown in the RGB ternary map we can decipher the following: White (High K, Th and U) zones are associated with exposed granitic bedrock and sediments derived from granite. The zones with white color represent promising targets for radioactive minerals exploration. Black to brown (Low in K, Th and U) zones is associated with diorite complex, older granites and sediments. Red zones are associated with an increase in the K

concentration. Green zones are associated with an increase in the Th concentration. Blue zones are associated with an increase in the U concentration. Cyan zones are high thorium and uranium with low potassium. Magenta parts are high potassium and uranium with low thorium. Finally, yellow parts are high potassium and thorium with low uranium. Some white (High K, Th and U) zones that had been mentioned to be associated with exposed granitic bedrock and sediments derived from granite are very much discriminated on the CMY map as all those rocks are now showing dark (black) color and can be mapped out. Whereas (Fig. 11) is a composite map of potassium (K) combining K (in red) with K/eTh (in green) and K/eU (in blue) and shows the total spatial distribution of relative concentrations of potassium.

On this map, high relative concentrations of potassium can be distinguished as anomalous, bright zones (high values). These anomalous zones correlate well with the granitoids. Due to differences in their chemical and physical properties of the rocks within the study area, the data can distinguish between different types of rock units (metasediments, metavolcanics and granitoids). Metavolcanics are associated with the dark zones on this image (low relative potassium values). However, metasediments

(Undifferentiated schists including phyllites) are associated with the light blue parts which occur along the western edge of the map. The major

structure labelled xx1 is also mapped out on (Fig. 11).

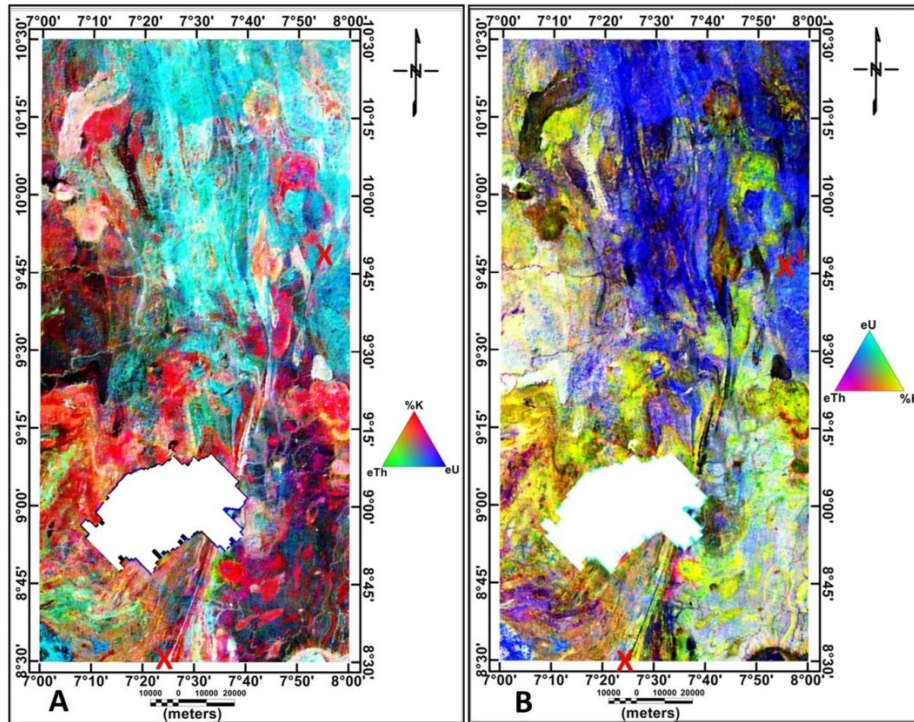


Fig. 10.a. Ternary (RGB) Map b. Ternary (CMY) Map (Fig. 12a)

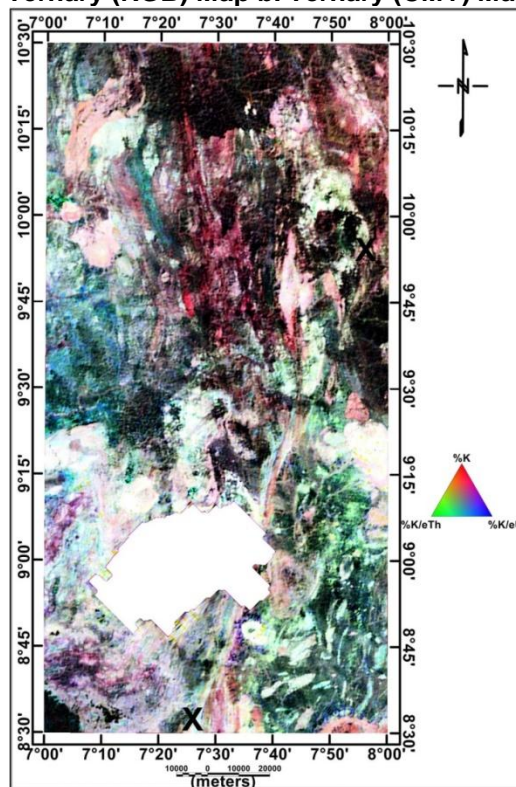
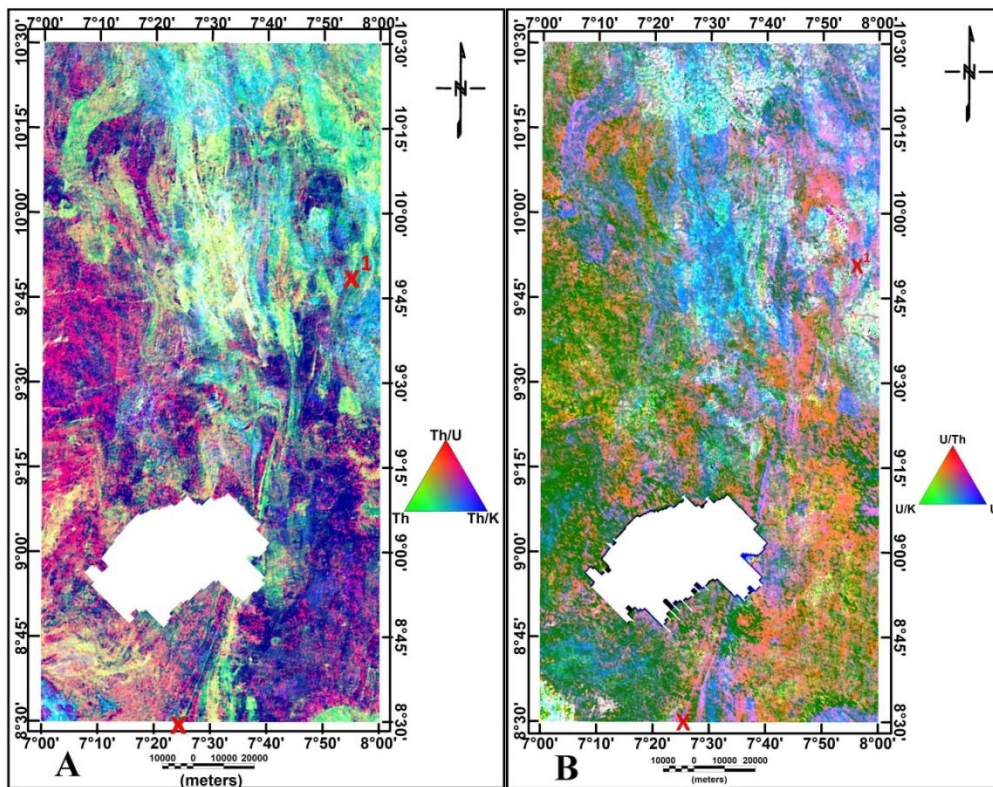


Fig. 11. a. Potassium Composite Map



**Fig. 12. a. Thorium composite map and b. Uranium composite map**

The composite image map of eTh (Fig. 12a) that combines eTh (green) with a ratio of eTh/eU (red) and eTh/K (blue) emphasizes the relative eTh distribution and highlights parts of thorium enrichment which is within the most elevated (north and north-eastern) part of the study area. Most prominent of the map is the paleostructure trending NE-SW marked xx<sup>1</sup> on the map.

According to [34], the relative concentration of eU for both K and eTh are important diagnostic factors in the recognition of possible deposits of uranium. The composite image map of eU (Fig. 12b) combines eU (blue) with ratio of eU/eTh (red) and eU/K (blue). This map could therefore help to identify the anomalous zones (bright areas on the image) of the uranium enriched concentration within the study area (Northeastern part of the map). Also, [10] put forward that the map may be useful in problems with geological mapping. Examination of this image shows that the high relative concentration of uranium (eU, eU / eTh and eU / K) is spatially correlated with migmatites and schists within the north and north-eastern part of the study area (Fig. 12b).

The main lithological units that represent different radioactivity levels were outlined using the

radioelement ternary images (Figs. 10a and 10b) and the surface geologic map of the study area was created using the identified lithological units (Fig. 13) while (Fig. 14) represent Hydrothermal alteration zone on surface geologic map delineated using radiometric data. From the map (Fig. 14), all the altered zones are observed to fall within granitic rocks which imply that alteration was principal as a result of the effect of hydrothermal fluid within the pre-existing rock that got altered.

### 3.6 Aeromagnetic and Aeroradiometric Data Integration

The results of aeromagnetic, aeroradiometric datasets and geology were integrated to produce a composite map of the study area (Fig. 15). A critical inspection of this map showed that the central portion of the study that is highly faulted coincided with the hydrothermal alteration zone that is located within the area. Also, several hydrothermally altered zones are mapped from the K/eTh ratio map (Fig. 10a). Since these zones have one or more structures associations, they serve as channels (pathways) for migrating hydrothermal fluids.

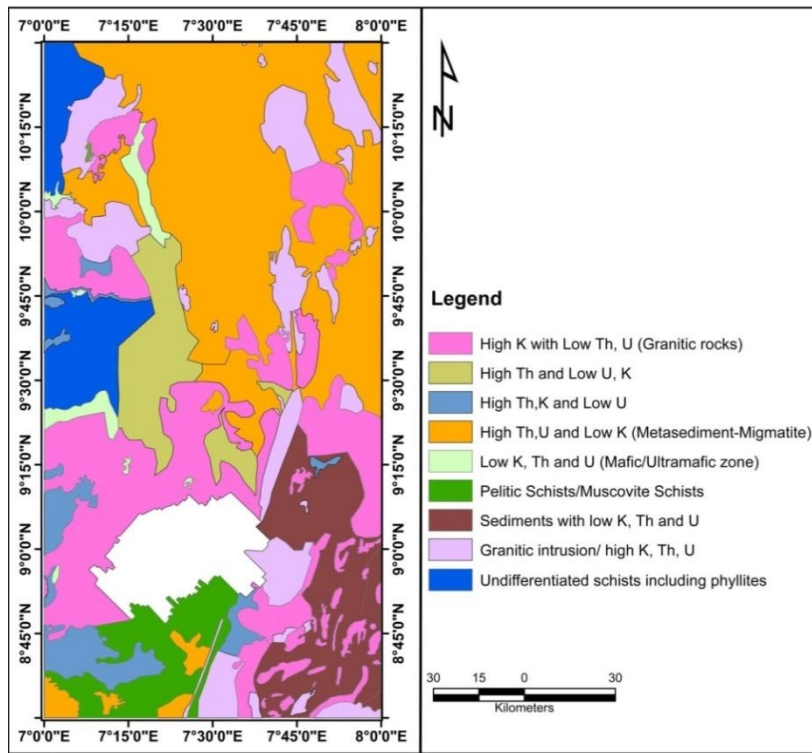


Fig. 13. Surface Geologic map of the Area from Aeroradiometric Data

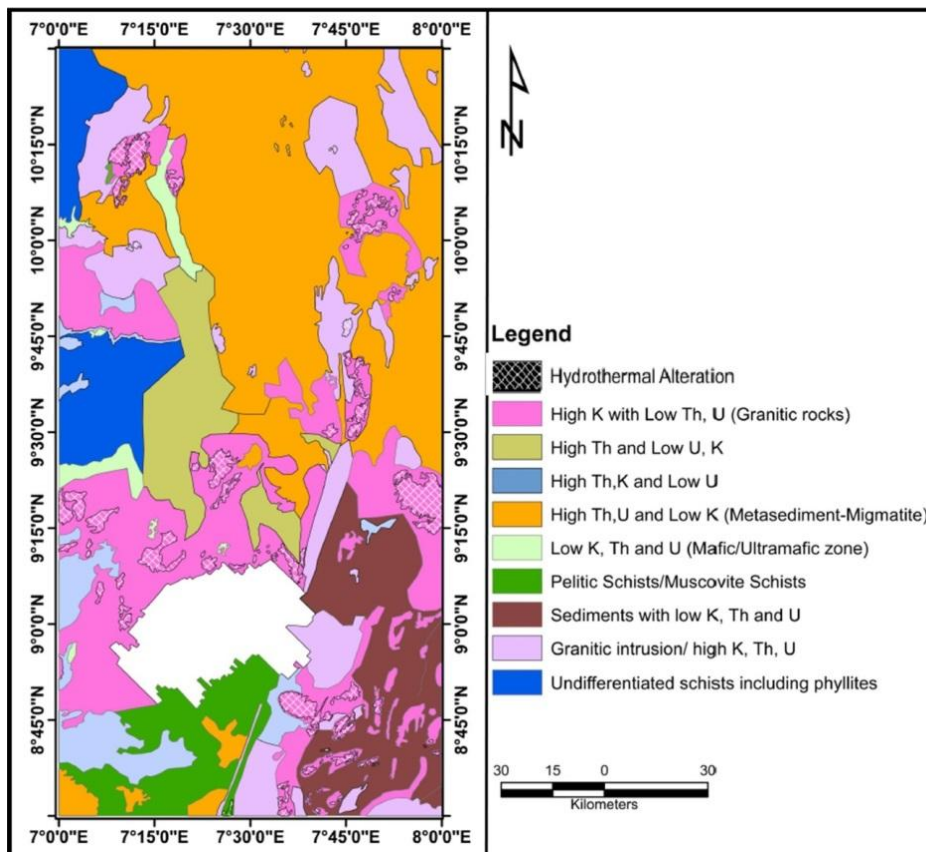


Fig. 14. Surface Geologic Map of the Area with Hydrothermal Alterations

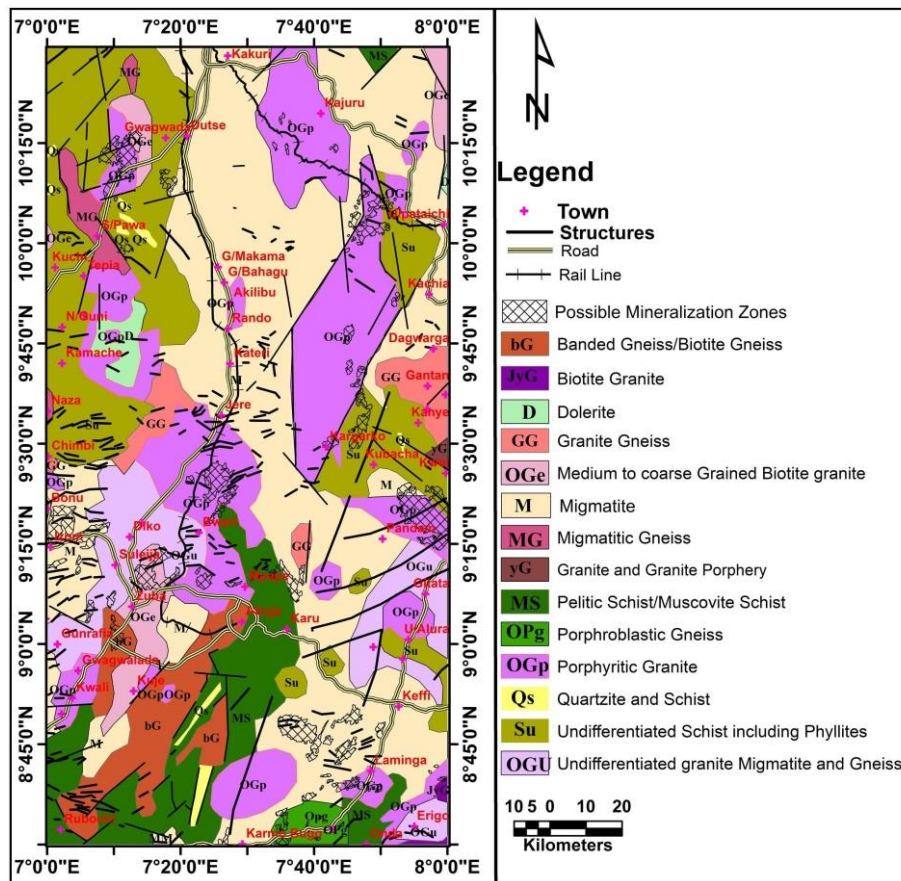


Fig. 15. Integrating hydrothermal alteration zones with geology and structures

#### 4. CONCLUSIONS

Zones characterized by the high K/eTh ratio values that are the strong indicator of hydrothermal alteration have been delineated (Figs. 9a). These are areas associated with younger granitoids and Metasediments in the eastern part of the study area. The alteration affected the porphyritic granite within the central portion of the map to the west (Figs. 9b). The migmatites within the edge of the map are highly affected by the hydrothermal alteration. Within the central portion of the map, medium to coarse-grained biotite granites were also affected by the hydrothermal alteration. Along the southeastern portion of the study area, there are isolated occurrences of hydrothermal alterations that spread across the Migmatite within this area. The resulting high K/eTh ratios, as observed within the study area, thus enables the distinction of potassium anomalies that have exploration significance from those related solely to lithological variations.

Ternary maps which are color composite images have been used to delineate the surface geologic

map of the study area (Fig. 13) since particular rock types often have characteristic ratios of the three radioactive elements, the ternary maps of these ratios are useful geological and mineral exploration tool for discriminating the zones of consistent lithology and contacts between contrasting lithology (Duval 1983). The ternary maps have aided in the delineation of the major structure labelled X to X<sup>1</sup> with trend NE-SW.

#### COMPETING INTERESTS

Authors have declared that no competing interests exist.

#### REFERENCES

1. Durrance EM. Radioactivity in geology: Principles and applications. Ellis Horwood Limited, Chichester, UK. 1986;441.
2. Ademila O, Akingboye AS, Ojamomi AI. The radiometric survey in geological mapping of parts of basement complex area of Nigeria: Vietnam Journal of Earth Sciences. 2018;40(3):288-298.

- DOI: 10.15625/0866-7187/40/3/12619
3. Mohamed ASY, Shadia TEI. (2013). Utilization of airborne gamma-ray spectrometric data for geological mapping, radioactive mineral exploration and environmental monitoring of southeastern Aswan city, South Eastern Desert, Egypt: *Geophysics Journal International*. 2013;195:1689–1700. DOI: 10.1093/gji/ggt375.
  4. Silva AM, McCafferty AE, Pires ACB. A new approach to map host rock for gold exploration in the Rio Das Velhas Greenstone Belt, Quadrilátero Ferrífero, Minas Gerais, Brazil. *Proceedings of the 6th International Congress of the Brazilian Geophysical Society*; 1999, CD.
  5. Darnley AG, Ford KL. Regional airborne gamma-ray surveys: a review, in *Proceedings of Exploration '87: Third Decennial International Conference on Geophysical and Geochemical Exploration for Minerals and Groundwater*, Special Volume No. 3, 960 pp, ed. Garland, G.D., Geological Survey of Canada. 1989;3.
  6. Davis JD, Guilbert JM. Distribution of the radioelements potassium, uranium and thorium in selected porphyry copper deposits. *Economic Geology and the Bulletin of the Society of Economic Geologists*. 1973;68(2).
  7. Elawadi E, Ammar A, Elsirafy A. Mapping surface geology using airborne gamma-ray spectrometric survey data - A case study. *Proceedings of SEGJ international symposium*. Nuclear Materials Authority of Egypt, Airborne Exploration Dept; 2004.
  8. Fertl WH. Gamma-ray spectral logging: a new evaluation frontier. *World Oil*. 1983; 79–91.
  9. Wedepohl KK. (Exec. Ed) *Handbook of Geochemistry*, Part 5, Berlin, Heidelberg, New York. 1978;2.
  10. Dickson BL, Scott KM. Interpretation of aerial gamma-ray surveys-adding the geochemical factors. *AGSO Journal of Australian Geology and Geophysics*. 1997;17(2):187–200.
  11. Ostrovskiy EA. Antagonism of radioactive elements in wallrock alteration fields and its use in aerogamma spectrometric prospecting. *International Geology Review*. 1975;17(4):461-468.
  12. Schwarzer TF, Adams JAS. Rock and soil discrimination by low altitude airborne gamma-ray spectrometry in Payne County, Oklahoma. *Economic Geology*. 1973;68: 1297-1312
  13. Lundien JR. Terrain analysis by electromagnetic means: Laboratory investigations in the 0- to 2.82 –MeV gamma-ray spectral region. U.S. Army Engineers Waterways Experiment Station, Vicksburg, Mississippi, Technical report 3–693. 1967;41.
  14. Hoover DB, Pierce AA. Annotated bibliography of gamma-ray methods applied to gold exploration; U.S. Geol. Surv. Open File. 1990;90-203.
  15. Nicolet JP, Erdi-Krausz G. Guidelines for radioelement mapping using gamma-ray spectrometry data; 2003.
  16. Moxham RM, Foote RS, Bunker CM. Gamma-ray spectrometer studies of hydrothermally altered rocks. *Economic Geology*. 1965;60;653-671.
  17. Bennett R. Exploration of hydrothermal mineralisation with airborne gamma-ray spectrometry; *Journal of Geochemical Exploration*, Canadian Institute of Mining and Metallurgy, Spec. 1971;11.
  18. Abdellatif MAG, Elkhateeb SO. Delineation of potential gold mineralisation zones in a part of Central Eastern Desert, Egypt using Airborne Magnetic and Radiometric data NRIAG *Journal of Astronomy and Geophysics*. 2018;7:361-376.
  19. Appiah D. Aeromagnetic and airborne radiometric data interpretation on Chirano area of the Sefwi Gold belt; A Master Thesis; 2015.
  20. Wemegah DD, Preko K, Noye RM, Boadi B, Menyeh A, Danuor SK, Amenyoh T. Geophysical interpretation of possible gold mineralization zones in Kyerano, South-Western Ghana using aeromagnetic and radiometric datasets. *J. Geosci. Environ. Prot*. 2015;3:67–82.
  21. Morrell AE, Locke CA, Cassidy J, Mauk JL. Geophysical characteristics of adularia-sericite epithermal gold-silver deposits in the Waihi-Waitekauri region New Zealand. *Econ. Geol*. 2011;106:1031–1041.
  22. Feebrey CA, Hishida H, Yoshioka K, Nakayama K. Geophysical expression of low sulfidation epithermal Au–Ag deposits and exploration implications-examples from the Hokusatsu region of SW Kyushu. *Jpn. Resour. Geol*. 1998;48:75–86.
  23. Irvine RJ, Smith MJ. Geophysical exploration for epithermal gold deposits. *J. Geochem. Explor*. 1990;36:375–412.

24. NGSA. Geology and Structural Lineament Map of Nigeria; 2006.
25. Obaje NG. Geology and Mineral Resources of Nigeria, Berlin: Springer-Verlag, Heidelberg. 2009;221.
26. Black R. Precambrian of West Africa. Episodes. 1980;4:3–8.
27. Tawey MD, Alhassan DU, Adetona AA, Salako KA, Rafiu AA, Udensi EE. Application of aeromagnetic data to assess the structures and solid mineral potentials in part of North Central Nigeria. Journal of Geography, Environment and Earth Science International. 2020;24(5):11-29.  
DOI:<https://doi.org/10.9734/jgeesi/2020/v24i530223>
28. Duval JS. Composite color images of aerial gamma-ray spectrometry data. Geophysics. 1983;48:722–735.
29. IAEA. Guidelines for radioelement mapping using gamma-ray spectrometry data, IAEA-TECDOC-1363, Vienna, Austria. 2003;179.
30. Broome HJ. Generation and interpretation of geophysical images with examples from the Rae Provinces, Northwestern Canada Shield, Geophysics. 1990;55(8):977–997.
31. Wilford JR, Bierwirth PN, Craig MA. Application of Airborne Gamma-ray Spectrometry in Soil/Regolith Mapping and Applied Geomorphology. AGSO Journal of Australian Geology and Geophysics. 1997;17(2):201-216.
32. Airo ML. Application of Aerogeophysical Data for Gold Exploration: Implications for Central Lapland Greenstone Belt. In: Ojala, J. V. (ed.) Gold in the Central Lapland Greenstone Belt, Finland. Geological Survey of Finland, Special Paper 44. 2007; 171–192.
33. Portnov AM. Specialization of rocks towards potassium and thorium in relation to mineralization; International Geology Review. 1987;29:326-344.
34. IAEA. Geochemical exploration for uranium. Technical Reports Series, No. 284, IAEA, Vienna, Austria. 1988;96.

© 2021 Tawey et al.; This is an Open Access article distributed under the terms of the Creative Commons Attribution License (<http://creativecommons.org/licenses/by/4.0>), which permits unrestricted use, distribution, and reproduction in any medium, provided the original work is properly cited.

*Peer-review history:*

*The peer review history for this paper can be accessed here:  
<http://www.sdiarticle4.com/review-history/67062>*